Nanoscale

Accepted Manuscript

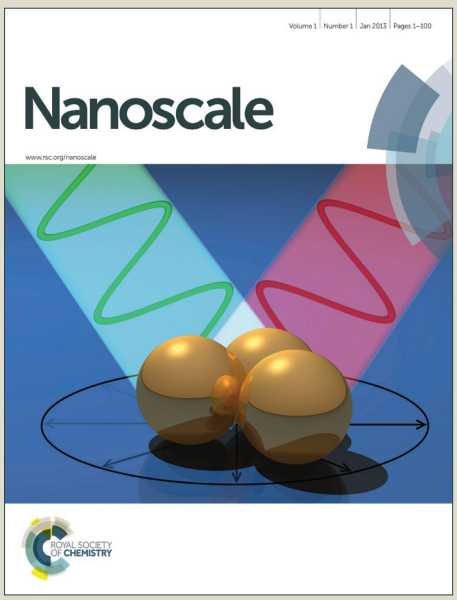

This is an *Accepted Manuscript*, which has been through the Royal Society of Chemistry peer review process and has been accepted for publication.

Accepted Manuscripts are published online shortly after acceptance, before technical editing, formatting and proof reading. Using this free service, authors can make their results available to the community, in citable form, before we publish the edited article. We will replace this *Accepted Manuscript* with the edited and formatted *Advance Article* as soon as it is available.

You can find more information about *Accepted Manuscripts* in the Information for Authors.

Please note that technical editing may introduce minor changes to the text and/or graphics, which may alter content. The journal's standard Terms & Conditions and the Ethical guidelines still apply. In no event shall the Royal Society of Chemistry be held responsible for any errors or omissions in this *Accepted Manuscript* or any consequences arising from the use of any information it contains.

ROYAL SOCIETY OF CHEMISTRY

www.rsc.org/nanoscale

Please do not adjust margins

Nanoscale

COMMUNICATION

Ultra-Sensitive Tandem Colloidal Quantum-Dot Photodetectors

Zhenyu Jiang,[a] Wenjia Hu,[b] Chen Mo,[a] Yan Liu,[a] Wenjun Zhang,[c] Guanjun You,[c] Li Wang,[a] Mahmoud R. M. Atalla,[a] Yu Zhang,[d] Jie Liu,[a] Kandhar K. Kurhade,[a] Jian Xu *[a]

Received 00th January 20xx,
Accepted 00th January 20xx

DOI: 10.1039/x0xx00000x

www.rsc.org/

The solution-processed PbSe colloidal quantum-dots (CQDs) infrared photodetector with tandem architecture is proposed to address the high dark current issue. The electrical transport mechanism in tandem has been fundamentally changed in which the recombination of carriers at intermediate layer becomes dominance rather than carriers hopping between nearest neighbors in CQD materials. As a result, the tandem photodetector exhibits ultra high detectivities of 4.7×10^{13} Jones and 8.1×10^{13} Jones under 34 μW/cm^2 illumination at 1100nm, at 275K and 100K, respectively.

High-performance, solution-processed colloidal quantum-dot (CQD) photodetectors (PDs) are of great interest due to low cost, low temperature processing, large device area and mechanical flexibility, which can hardly be achieved by PDs made of epitaxially grown crystalline semiconductors [1]. In addition, the bandgap of CQDs is tunable over a broad spectral range from visible to near-infrared (NIR), making them attractive for visible and NIR sensing applications. G. Konstantos et al. [2] reported a photoconductor device based on PbS CQDs with normalized detectivities of ~10^{13} Jones at 40V bias. However, the lateral conduction path design requires large driving voltage which is often too high to be compatible with conventional electronic driver circuitry unless additional voltage amplifier is used. J.P. Clifford et al.[3] reported a low-bias (~0V) PbS CQD NIR photodiode device with a normalized detectivity around ~10^{12} Jones at 250K operation temperature. In either cases the dark current noise was inevitably high due to the narrow bandgap and high density of surface states of PbSe CQDs, which has become the main limiting factor for the CQD detector performance. One approach is to increase the interparticle coupling and mobility by replacing the long insulating oleate ligands with shorter and more conductive surfactant molecules, such as ethanedithiol (EDT) and benzenedithiol (BDT) [4,5]. Nevertheless, this approach is often insufficient to resist the dark current [6]. The other strategy is to suppress the charge injection with carrier blocking layers [6]. But this technique often pinches off the dark current and the photocurrent at the same time, because the blocking mechanism applies equally to the thermally excited carriers and the optically excited carriers.

In this work, we address the high-dark current drawback by proposing a novel tandem architecture for the solution-processed NIR CQD PDs. The tandem architecture implements ZnO and Poly[N,N'-bis(4-butylphenyl)-N,N'-bis(phenyl)- benzidine] (poly-TPD) intermediate layer in between two cascaded PbSe CQD active (absorber) layers. The unique merit for the tandem PD is that the intermediate layer functions as effective energy barrier that blocks the dark current leakage, whereas the photocurrent is harvested via high-efficiency carrier recombination at the intermediate layer. In doing this, the role of the CQD material itself played in electrical transport mechanism has no longer been the major limiting factor for the detector performance. The measured dark current of the tandem PD exhibits a drastic reduction of more than three orders of magnitude compared to that of the PD with a single active layer (In the following context, it will refers to single-layer PD unless otherwise noted), which is also accompanied with an elevated photocurrent. Under -0.1V bias, the tandem photodetector has achieved ultra high detectivities up to 4.7×10^{13} and 8.1×10^{13} Jones at 275K and 100K respectively. The low-temperature current-voltage (I-V) characteristics reveals that the carrier recombination at the intermediate layer plays the key role in the electrical transport mechanism of the CQD tandem PDs under study. Our results validate the effectiveness of dark current blocking in tandem CQD PDs and opens up a new avenue to further suggest that the tandem architecture can be employed to develop high-performance solution-processed light detection devices.

PbSe CQDs, ZnO, poly-TPD were dissolved in chlorobenzene, ethanol and chlorobenzene with concentration of 20, 15 and 15mg/ml respectively. The solutions were prepared and stored inside the nitrogen glovebox. PbSe CQDs were synthesized following the non-coordinating solvent technique developed by Yu [7]. The ZnO nanocrystals (NCs) were synthesized through the sol-gel method [8]. The patterned ITO glass substrates (sheet resistance ~15Ω/□) were cleaned sequentially by ultrasonicating in de-ionized water, acetone and IPA for 15 minutes each, and then exposed to

[a] Department of Engineering Science and Mechanics, Pennsylvania State University, University Park, PA, 16802, USA.
[b] China Tianchen Engineering Corporation, Tianjin, 300400, China.
[c] Shanghai Key Lab of Modern Optical System, University of Shanghai for Science and Technology, Shanghai, 200093, China.
[d] State Key Laboratory on Integrated Optoelectronics and College of Electronic Science Engineering, Jilin University, Changchun, 130012, Chin.
* corresponding author, Email: jianxu@engr.psu.edu
See DOI: 10.1039/x0xx00000x

Nanoscale Accepted Manuscript

Please do not adjust margins

UV-zone for 15 minutes. The poly (ethylenedioxythiophene):polystyrenesulphonate (PEDOT:PSS) (30 nm thick) was spin-coated on top of ITO glass followed by thermal annealing at 150℃ for 15 minutes. Then the substrates were immediately transferred to glove box for rest process. PbSe QDs films were spin-coated and treated with 1,2-Ethanedithol (EDT) according to the same procedure described in our previous work [9]. ZnO NCs, poly-TPD, PbSe CQDs, ZnO NCs were spin-coated and annealed for 30 minutes at 80℃ for each layer. The thickness of the PbSe CQD layer, ZnO NCs layer, poly-TPD layer were 75nm, 40nm, 45nm, respectively. Finally, the devices were completed by thermally evaporating 150nm-thick aluminum layer as the cathode and encapsulated for further characterization. The area of the devices is 2×2 mm^2. The low temperature electrical transport measurements were carried out in a liquid He cryostat system. The current-voltage (I-V) characteristics of the photodetectors were measured with a Keithley 2612 analyzer, a 650nm laser diode was used to obtain the photocurrent. To obtain the spectral response of the photodetectors, the devices were irradiated under monochromatic light through Newport monochromator using a xenon lamp as the light source. The illumination intensities were measured using calibrated Newport 818 and Newport 818IR detectors for visible and infrared range, respectively. The intensity of incident light was tuned by using a set of attenuators.

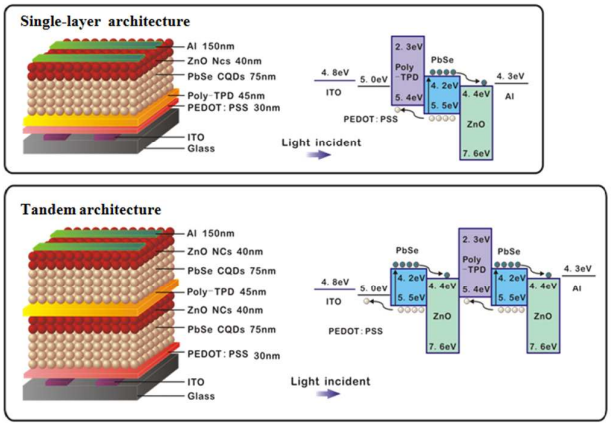

Figure 1: Device architectures and band diagrams of single-layer and tandem photodetectors.

Figure 1 shows the architecture and simplified band diagram of the tandem PD: Glass/ITO/poly(ethylenedioxythiophene):polystyrenesulphonate (PEDOT:PSS)/PbSe CQDs/ZnO/ (poly-TPD) /PbSe CQDs/ZnO/Al. The ZnO hole blocking layer (HBL) and the poly-TPD electron blocking layer (EBL) are used as intermediate layer to connect and separate the bottom (in front of the light illumination) and the top (back) detectors. The intermediate layer is used as a recombination center allowing the recombination of the electrons from one sub-detector with the holes from the other detector. The tandem PD employs the PbSe CQDs of the same bandgap for bottom and top active layers, ensuring the sensitivity to a monochromatic light wavelength. The simplified band diagram in **figure 1** illustrates the electrical transport mechanism of the tandem PD. The thermal or optical generated electron-hole (e-h) pairs are separate at the junctions of both sub-detectors. The holes from bottom detector are captured by the anode and electrons from top detector are collected by the cathode; meanwhile the electrons from the bottom detector recombine with holes from the top detector at ZnO/poly-TPD interface. Therefore, the carrier transportation is determined by the recombination at the interface of ZnO and poly-TPD. As a result, the recombination of electrons and holes at ZnO/poly-TPD interface of the tandem architecture functioning as a valve brings more possibilities to manipulate the current flow.

As a control, **figure 1** also shows the architecture and simplified band diagram of the single-layer PD: Glass/ITO/PEDOT:PSS/poly-TPD/PbSe CQDs/ZnO/Al. The e-h pairs generated at PbSe layer via thermal or optical excitation will be separated at the PbSe/ZnO junction by the built-in potential or the reverse bias. Holes go through the poly-TPD can be captured by anode and electrons go through the ZnO can be captured by cathode. Virtually no energy barrier present at the transport pathways, thus the single-layer architecture is unlikely to suppress the dark current leakage. As a result, single-layer CQD PDs have been suffered from high leakage dark current originating from CQD materials.

An important figure of merit is specific detectivity (D^*) which utilized to characterize the sensitivity of a PD. At high frequency where 1/f noise is negligible, the shot noise limited D^* is given by [10-12]:

$$D^* = \frac{R_\lambda}{\sqrt{2qJ_d+(4kT/AR_d)}} \qquad (1)$$

where R_λ is the responsivity at wavelength λ, q is the elementary charge, J_d is the dark current density in Acm^{-2}, A is the device area, R_d is the dynamic resistance.

Figure 2a shows the dark and photo I-V characteristics of the single-layer and tandem PDs. The photocurrents were measured under 37.5mW/cm^2 illumination at 650nm. The dark current of the tandem PD drops more than three orders of magnitude than that of the single-layer PD, whereas the photocurrent is slightly greater than that of the single-layer PD. The rectification ratios of the single-layer and tandem PDs at +/-1V are 5 and 1.2×10^4, respectively. The small rectification ratio of the single-layer PD is due to a large density of trapped states present at the surface of CQDs which serve as transport pathways and recombination centers [13,14]. **Figure 2**b shows the responsivities and calculated shot noise limited detectivities of the single-layer and tandem PD as a function of reverse bias under 37.5mW/cm^2 illumination at 650nm. The R_λ of the tandem PD is greater than that of the single-layer PD, and D^* shows nearly two orders of magnitude improvement. For tandem PD at -0.5V bias, R_λ=0.36 A/W, $D^*=1.4\times10^{12}$ Jones, the detectivities are over 10^{13} Jones when approaching to 0V. The external quantum efficiency (EQE) at -0.5V is η_{ext}=69% which indicates high recombination efficiency at the poly-TPD/ZnO interface. The detectivity spectrum has also been investigated. **Figure 3**a shows the absorption spectra of PbSe CQD materials in solution as-synthesized and in film after EDT treatment. A red-shift was observed after EDT treatment because of the change in oscillator strength and dipole–induced dipole coupling arising from the densification of the PbSe CQD film [5]. **Figure 3**b shows the calculated detectivities of single-layer and tandem PDs as a function of wavelength at -0.5V bias. The detectivity spectrum

Nanoscale Accepted Manuscript

This journal is © The Royal Society of Chemistry 20xx

corresponds closely to the absorption spectrum. The detectivities of tandem PDs exhibit nearly two orders improvement than that of single-layer PDs, and are greater than 6.7×10^{11} Jones at wavelengths from 450nm to 1200nm with an excitonic peak value 1.1×10^{12} at 1120nm. These results demonstrate that the tandem PD has successfully suppressed dark current and exhibited much better detector performance.

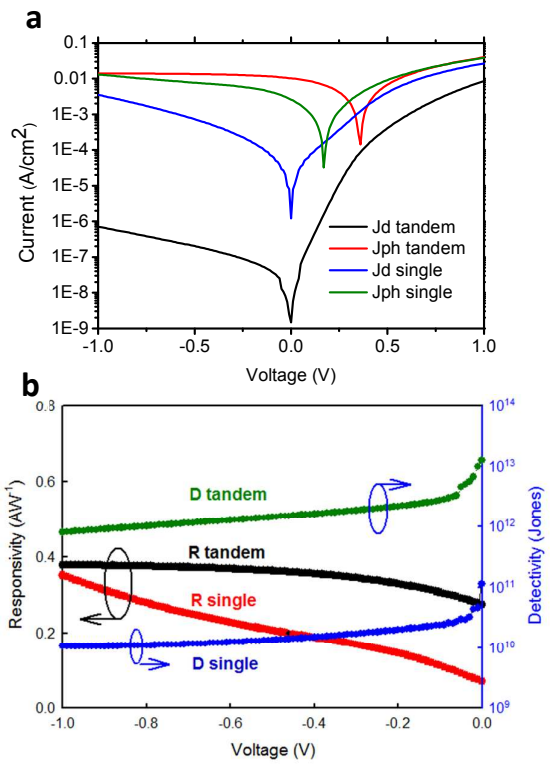

Figure 2a: Dark (J_d) and photo (J_{ph}) current-voltage (I-V) characteristics of single-layer and tandem photodetectors. **2b**: Responsivities and calculated shot noise limited detectivities as a function of voltage for single-layer and tandem and photodetectors.

The photocurrent of tandem photodetectors is determined by the recombination efficiency of electrons and holes at the intermediate layer similar to that of tandem solar cells. The carrier balance between bottom and top detectors is critical to obtain high photocurrent. To examine this hypothesis, we set the thickness of the bottom PbSe CQD layer as constant (75nm), and the thickness of the top PbSe CQD layers as 50nm, 75nm and 100nm, for device A, B and C, respectively. **Figure 4** shows the responsivities of these three devices over visible and infrared wavelength range. The device A exhibits the lowest responsivity over the entire spectrum, which justifies that the imbalance of carriers results in insufficient recombination at ZnO/poly-TPD interface, which cause low responsivity at given illumination power. When the thickness of the top PbSe CQD layer increased to 75nm, the responsivity increased accordingly because more carriers generated in the top detector which lead to more e-h recombined at intermediate layer. Moreover, the responsivity is saturated if the thickness of the top PbSe CQD layer further increased to 100nm. This saturation phenomenon demonstrates that the photocurrent of the tandem PD is subjected to the sub-detector with less number of carriers generated, which verified our hypothesis that the photocurrent harvest is due to the high recombination efficiency of carriers at the intermediate layer.

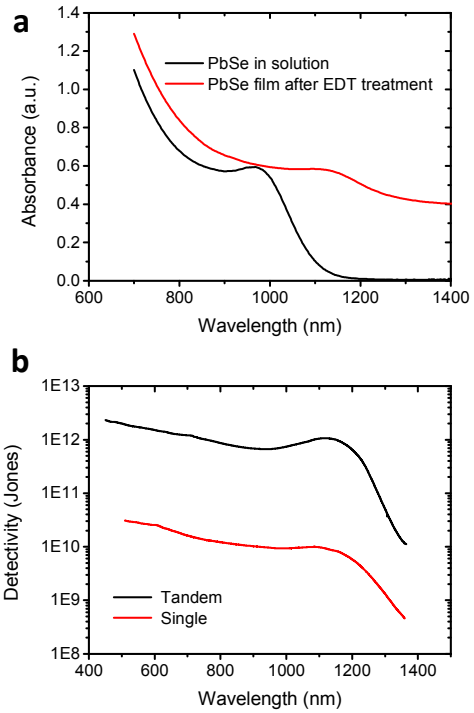

Figure 3a: Absorption spectra of PbSe CQDs solution and PbSe CQD film after EDT treatment. **3b**:Shot noise limited detectivities across the visible and IR wavelengths of tandem and single-layer photodetectors at -0.5V bias.

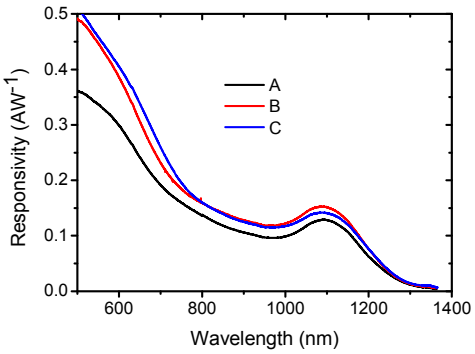

Figure 4: Responsivity spectra across visible and IR wavelengths of tandem photodetectors with different top PbSe CQD film thickness (50, 75 and 100 nm for device A, B and C, respectively).

To further understand the electrical transport mechanism underpinning single-layer and tandem architecture, low temperature I-V characteristics have been investigated. The electrical transport of CQD-based devices can be described by disordered system which conductance, *G(T)*, is given by [15]:

$$G(T)=G_0 exp[-(T_0/T)^p] \quad (2)$$

Nanoscale Accepted Manuscript

where the pre-exponential factor G_0 is independent of temperature (T) or a slowly varying function of T, T_0 is a constant of the material. The value of p, ranging from 1/4 to 1, depends on the temperature range and the nature of the transport process of the devices.

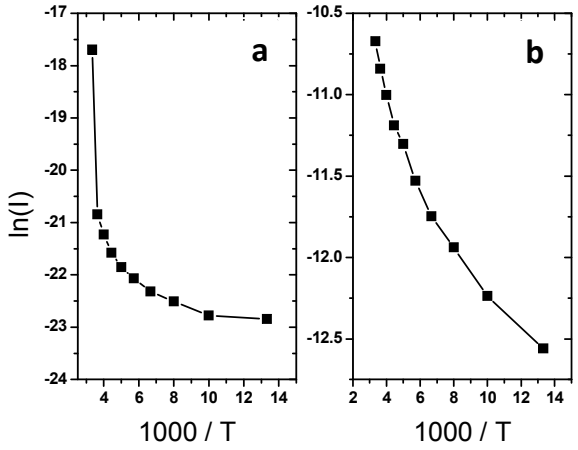

Figure 5a: ln(I) as a function of inverse T for single-layer photodetectors at -0.5V bias. **5b**: ln(I) as a function of inverse T for tandem photodetectors at -0.5V bias.

The dependence of *ln(I)* at -0.5V bias on the inverse of absolute T for single-layer and tandem PDs are shown in **Figure 5a** and **5b**, respectively, where I is the measured current. Several distinct regions are clearly observed which similar to disordered semiconductors. The observed Arrhenius-like dependence ($p=1$) for both single-layer and tandem PDs near room temperature (275K~300K, 3.33~3.64 on 1000/T scale) is related to a thermally activated transport process. *Equation 2* can be reduced to $G=G_0exp(-E_a/k_BT)$, where E_a is the activation energy for charge transport. From the slope of the Arrhenius plots we found E_a~48.5 meV for the single-layer PD. This value is in agreement with other single-layer PbSe CQD devices where E_a~ 25 meV [16], ~52.2 meV [17] and ~95 meV [18], respectively. The bandgap of PbSe CQDs is E_g~1.3eV, which means the carrier density of thermally excited CQDs is negligible and the electrical transport mainly originates from carriers hopping between nearest neighbors (NNH) [18]. In contrast, E_a found to be 0.89 eV for tandem PDs near room temperature. In intrinsic semiconductor materials where the transport mechanism dominated by generation-recombination process, $E_a=E_g/2+\Delta E$, where ΔE is the Coulomb barrier [18]. The activation energy of the tandem photodetector is in reasonable agreement with E_g~1.3eV, which means it possesses an intrinsic generation-recombination transport arising from the thermal activated carriers across bandgap at two active PbSe CQD layers which annihilated by recombining with each other at intermediate layer. Thus the NNH transport in PbSe CQD material becomes negligible in the tandem photodetectors. On the other hand, the tremendous increase in the activation energy of tandem PDs also indicates an effective energy barrier present at tandem PDs, which eventually blocks the leakage current. The T dependence of the photocurrent at 650nm light illumination has also been investigated, the activation energy found to be E_a~72 meV at near room temperature. We speculate that the much smaller activation energy of the photocurrent is probably due to the charge accumulation at the poly-TPD/ZnO interface that enables field-assisted recombination. As a result, the dark current blocking and photocurrent harvesting can occur simultaneously in tandem PD device. At lower temperature (<200K), a much slower decreasing of dark current has been observed for both single-layer and tandem PDs which indicate the dominance of other electric transport mechanisms, probably Efros-Shklovskii variable-range hopping (ES-VRH) (p=1/2), or Mott-variable-range-hopping (M-VRH) (p=1/4) [15, 18, 19].

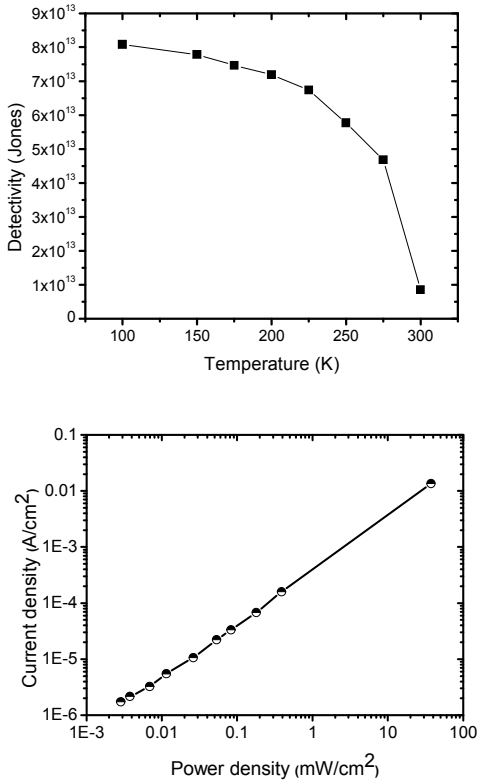

Figure 6a: Shot noise limited detectivities of the tandem photodetector under 34 μW/cm^2 illumination at -0.1V at 1100nm wavelength as a function of temperature. **6b**: Photo current density of the tandem photodetector as a function of illumination intensities.

Figure 6a shows the specific detectivities of the tandem photodetector under 34 μW/cm^2 illumination at -0.1V at 1100nm and various temperature. The D^* value is increased with the decreasing of operating temperature. The D^* achieved 8.6×10^{12} Jones at 300K, 4.7×10^{13} Jones at 275K and 8.1×10^{13} Jones at 100K, respectively, which are comparable to other CQD-based NIR photodetectors [2,3,6].

Another figure of merit for PDs is the linear dynamic range (LDR), also known as photosensitivity linearity (typically quoted in dB), LDR is given by [12]:

$$LDR=20log(J^*_{ph}/J_d) \quad (3)$$

where J^*_{ph} is the photocurrent measured at light intensity of 1 mW/cm^2. **Figure 6b** shows the linearity of the tandem photodetector at -0.5V bias under 650nm illumination. Good

Nanoscale Accepted Manuscript

This journal is © The Royal Society of Chemistry 20xx

linearity has been observed from 2.85 μW/cm^2 to 37.5 mW/cm^2. Under -0.5V bias the LDR at 650nm and 1100nm are 66dB and 64dB repectively. These values are equal or close to that of InGaAs PDs (66dB) [12]. When comes to smaller reverse bias, the LDR of the tandem photodetector will give higher LDR value.

Conclusions

In summary, we implemented the tandem architecture to block dark leakage current of PbSe CQD infrared photodetectors. The tandem architecture fundamentally changed the electrical transport mechanism in which carrier recombination at the poly-TPD/ZnO plays a much important role than the NNH in CQD materials. As a result, the performance of the tandem PDs has been greatly enhanced in regardless of the intrinsic unfavorable properties of the CQD materials, which rendering the tandem architecture as a promising design for developing ultra-sensitive solution-processed photodetectors.

Acknowledgements

The authors thank Prof. Stephen Fonash and Prof. John Asbury for their help during the course of study. The work at the Penn State University is supported by the National Science Foundation under grants ECCS0846018 and ECCS0824186.

References

1 Z. Jiang, G. You, L. Wang, J. Liu, W. Hu, Y. Zhang, J. Xu, *J. Appl. Phys*., **2006**, 116, 084303.
2 G. Konstantaos, I. Howard I, A. Fischer, S. Hoogland, J. Clifford, E. Klem, L. Levina, E.H. Sargent, *Nature*, **2006**,442, 180.
3 J.P. Clifford, G. Konstantatos, K.W. Johnston, S. Hoogland, L. Levina, E.H. Sargent, *Nature Nanotechnology*, **2009**, 4, 40.
4 M. Law, J.M. Luther, Q. Song, B.K. Hughes. C.L. Perkins, A.J. Nozik, *J. Am. Chem. Soc.*, **2008**, 130, 5974.
5 J. M. Luther, M. Law, Q. Song, C.L. Perkins, M.C. Beard, A.J. Nozik, *ACS Nano*, **2008**, 2, 271.
6 G. Sarasqueta, K.R. Choudhury, J. Subbiah, F. So, *Adv. Funct. Mater*.**2011**, 21, 167.
7 W.W. Yu, J.C. Falkner , B.S. Shih, V.L. Colvin, *Chemistry of Materials*, **2004**, 16, 3318.
8 J. Bang, H. Yang, P.H. Holloway, *Nanotechnology*, **2006**, 17, 973.
9 W. Hu, R. Henderson, Y. Zhang, G. You, L. Wei, Y. Bai, J. Wang, J. Xu, *Nanotechnology*, **2012**, 23, 375202.
10 A. Jha, Infrared Technology (Wiley, New York, **2000**.), pp. 245-359.
11 P. Bhattacharya, Semiconductor Optoelectronics Device (Prentice-Hall, Upper Saddle River, NJ, **1997**), pp. 245-367.
12 X. Gong, M. Tong, Y. Xia, W. Cai, J.S. Moon, Y. Cao, G. Yu, C. Shieh, B. Nilsson, A.J. Heeger, *Science*, **2009**, 325, 1665.
13 M.B. Jarosz, V.J. Porter, B.R. Fisher, M.A. Kastner, M.G. Bawendi, *Phys. Rev. B* **2004**, 70, 195327.
14 D.S. Ginger, N.C. Greeham, *J. Appl. Phys.***2000**, 87, 1361.
15 N.F. Mott, E.A. Davis, *Electronic Processes in Non-Crystalline Materials* (Clarendon, New York, **1979**).
16 G. Sarasqueta, K.R. Choudhury, F. So, *Chem. Mater.***2010**, 22, 3496.
17 G. Dedigamuwa, J. Lewis, J. Zhang, X. Jiang, P. Mukherjee, Witanachchi S.; *Appl. Phys. Lett.***2009**, 95, 122107.
18 H.E. Romero, M. Drndic, *Phys. Rev. Lett.***2005**, 95, 156801.
19 M. S. Kang, A. Sahu, D. J. Norris, C. D. Frisbie, Nano Lett., **2011**, 11(9), 3887-3892.

Nanoscale Accepted Manuscript